Available online at www.sciencedirect.com
SCIENCE DIRECT®
Chemical Physics 298 (2004) 251–261
Chemical Physics
www.elsevier.com/locate/chemphys

Ultrafast excited state dynamics of the bi- and termolecular stilbene-viologen charge-transfer complexes assembled via host–guest interactions

E.N. Ushakov [a,*], V.A. Nadtochenko [a], S.P. Gromov [b], A.I. Vedernikov [b], N.A. Lobova [b], M.V. Alfimov [b], F.E. Gostev [c], A.N. Petrukhin [c], O.M. Sarkisov [c]

[a] *Institute of Problems of Chemical Physics, Russian Academy of Sciences, Chernogolovka 142432, Russia*
[b] *Photochemistry Center of the Russian Academy of Sciences, Novatorov str. 7A, Moscow 119421, Russia*
[c] *N.N. Semenov Institute of Chemical Physics, Russian Academy of Sciences, Kosygin str. 4, Moscow 117977, Russia*

Received 5 September 2003; accepted 3 December 2003

Abstract

Excited state dynamics of the highly stable 1:1 and 2:1 charge-transfer (CT) complexes assembled via host–guest interactions between a biscrown stilbene and a viologen vinylog was studied using transient pump-supercontinuum probe spectroscopy. In acetonitrile, both complexes showed ultrafast two-component transient absorption dynamics after excitation in the CT absorption band by a 616 nm, 70 fs laser pulse. The faster component ($\tau < 200$ fs) is assigned to relaxation processes in the lowest CT excited state. The second component is due to the back electron transfer (ET) reaction leading to the ground state. The measured ET time constants for the 1:1 and 2:1 CT complexes are about 540 fs and 1.08 ps, respectively. Excitation of the bimolecular complex by a 308 nm laser pulse gave rise to three-component transient absorption dynamics. The fastest transient ($\tau \sim 150$ fs) is assigned to relaxation processes in the high-lying excited states of the complex. The high-amplitude rise component with a time constant of about 300 fs is due to the internal conversion from the high-lying excited states to the lowest CT excited state. The latter decayed to the ground state via the back ET with a time constant very close to that measured when the complex was excited in the CT absorption band.

Keywords: Biscrown stilbene; Viologen vinylogs; Supramolecular donor–acceptor complexes; Femtosecond transient absorption dynamics; Electron transfer; Vibrational relaxation; Internal conversion

1. Introduction

Electron transfer (ET) reactions play an important role in many chemical, physical and biological systems [1,2]. Accordingly, ET dynamics is one of the broadest research areas of physical chemistry. Organic charge-transfer (CT) complexes [3] are widely used as model systems for studies of ET dynamics. These complexes undergo direct photoinduced ET reaction upon excitation in the CT absorption band. Until now there are some issues concerning the back ET reaction (charge recombination) in excited organic CT complexes. Many evidences have been reported [4–6] that the semiclassical nonadiabatic ET theory fails to describe satisfactorily the Gibbs free energy dependence of the back ET rate constant. To account for these discrepancies, a few extensions of the nonadiabatic ET theory have been proposed; such as the hybrid model of Barbara and co-workers that includes both high-frequency quantum mode and solvent coordinate [7,8]. For some CT complexes, this model qualitatively well describes the free energy dependence of the ET rate [9]. Recently, the hybrid model has been extended to include the effects of internal vibrational relaxation [10]. However, the

* Corresponding author. Address: Department of Photochemistry, Institute of Problems of Chemical Physics of RAS, Institutskii prospect 18, 142432 Chernogolovka Moscow region, Russia. Tel.: +7-096-524-4746; fax: +7-096-515-5420.
E-mail address: eushakov@icp.ac.ru (E.N. Ushakov).

0301-0104/$ - see front matter © 2003 Elsevier B.V. All rights reserved.
doi:10.1016/j.chemphys.2003.12.002

nonequilibrium ET models predict a nonexponential ET dynamics, which is inconsistent with the observations reported in [4–6,9].

Generally, molecules in organic CT complexes are weakly bound, which complicates studies of the excited state dynamics. Recently, the highly stable CT complex $[\mathbf{S}\cdot\mathbf{V}]^{4+}$ ($\log K = 9.08$ in acetonitrile) between the biscrown stilbene **S** and the viologen-like salt $\mathbf{V}^{4+}$ (Scheme 1) has been reported [11].

The high thermodynamic stability of $[\mathbf{S}\cdot\mathbf{V}]^{4+}$ is provided by the two-centre host–guest bonding between the peripheral fragments of the electron donor (D) **S** and the electron acceptor (A) $\mathbf{V}^{4+}$, as illustrated in Scheme 1. The host–guest bonding in $[\mathbf{S}\cdot\mathbf{V}]^{4+}$ places some constraints on both the donor–acceptor separation distance and the spatial orientation of the donor and acceptor moieties. Owing to these advanced features, supramolecular CT complexes of the $[\mathbf{S}\cdot\mathbf{V}]^{4+}$ type are attractive model systems for studies of ET process.

More recently [12], it has been found that compounds **S** and $\mathbf{V}^{4+}$ in acetonitrile are able to form the termolecular CT complex $[\mathbf{S}\cdot\mathbf{V}\cdot\mathbf{S}]^{4+}$ ($\log K = 12.28$, Scheme 1), which has a sandwich-type layered structure in which the acceptor salt is located between two complexed molecules of the biscrown stilbene. ET process in termolecular CT complexes is not clearly understood because these species normally show a very low thermodynamic stability and exist in solution in equilibrium with CT complexes of other compositions. In addition, there is an element of uncertainty about symmetry of termolecular CT complexes, e.g. for 2:1 donor–acceptor complexes both the symmetrical D–A–D and asymmetrical D–D–A structures are theoretically possible. With **S** and **V**, the equilibrium is completely shifted toward the symmetrical D–A–D complex $[\mathbf{S}\cdot\mathbf{V}\cdot\mathbf{S}]^{4+}$ when **S** is added to a solution of the D–A complex $[\mathbf{S}\cdot\mathbf{V}]^{4+}$ in an excess of ~0.05 M. No higher-order CT complexes, i.e. those involving more than three components, are formed in this system. Studies of the excited state dynamics of the termolecular complex $[\mathbf{S}\cdot\mathbf{V}\cdot\mathbf{S}]^{4+}$ might give new knowledge about ET process in symmetrical D–A–D complexes.

Here, we report results of femtosecond transient absorption spectroscopy studies of the supramolecular CT complexes $[\mathbf{S}\cdot\mathbf{V}]^{4+}$ and $[\mathbf{S}\cdot\mathbf{V}\cdot\mathbf{S}]^{4+}$ in acetonitrile. Transient spectroscopy data for the uncomplexed compounds **S** and $\mathbf{V}^{4+}$, as well as for the reference viologen salt $\mathbf{EV}^{2+}$ are also presented.

2. Experimental

Trans-1,2-bis[2,3,5,6,8,9,11,12,14,15-decahydro-1,4,7,10,13,16-benzohexaoxacyclooctadecin-18-yl]-ethylene **S**, *trans*-1,2-bis[1-(3-ammoniopropyl)-4-pyridiniumyl]-ethylene tetraperchlorate $\mathbf{V}^{4+}$, and *trans*-1,2-bis[1-ethyl-4-pyridiniumyl]-ethylene diperchlorate $\mathbf{EV}^{2+}$ were prepared as described previously [11]. Complex $[\mathbf{S}\cdot\mathbf{V}]^{4+}$ was obtained by mixing of equimolar amounts of **S** and $\mathbf{V}^{4+}$ in a minimal volume of acetonitrile. The complex was precipitated by slow saturation of its solution with benzene at ambient temperature. The solid residue was recrystallized under the same conditions, and then filtered and dried on the air. This procedure afforded complex $[\mathbf{S}\cdot\mathbf{V}]^{4+}$ in almost quantitative yield.

Samples were dissolved in acetonitrile and studied at ambient temperature. Solutions of $[\mathbf{S}\cdot\mathbf{V}\cdot\mathbf{S}]^{4+}$ were made by adding of **S** to solutions of $[\mathbf{S}\cdot\mathbf{V}]^{4+}$ in an excess of 0.05 M over the 1:1 complex. Commercially available

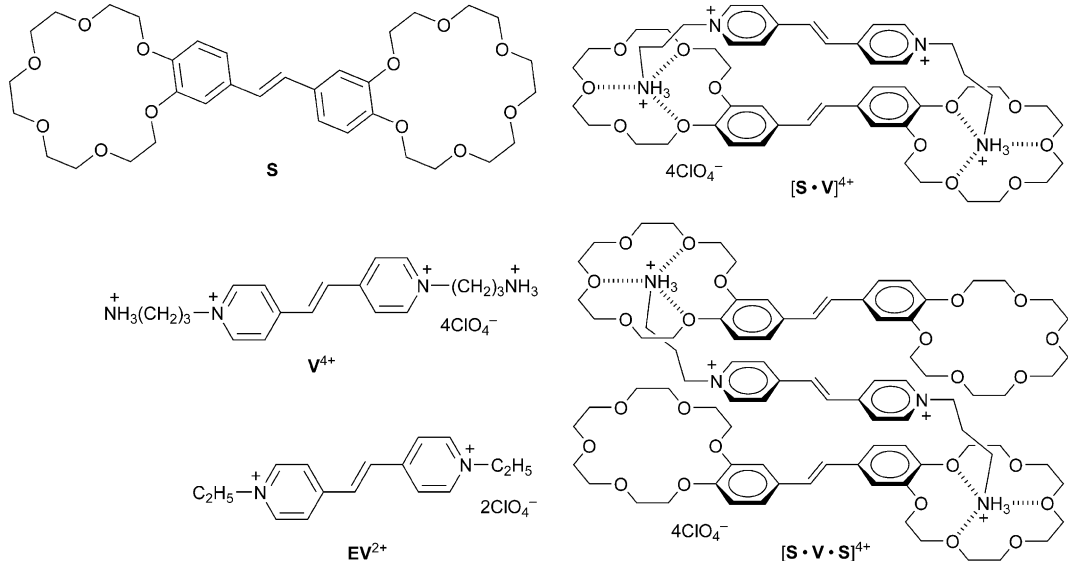

Scheme 1.

anhydrous acetonitrile ($H_2O < 0.01\%$) of spectrophotometric grade was used as received.

Steady-state absorption and emission spectra were recorded on standard laboratory instruments. Quantum yields of *trans* → *cis* photoisomerization were measured upon steady-state irradiation by glass-filtered 313 nm light of a high-pressure Hg lamp. Light intensity was measured by a cavity receiver, giving an error in the quantum yield measurements of ~20%. Emission quantum yields were determined using anthracene in ethanol as standard ($\varphi_f = 0.28$).

Transient absorption spectra were measured using the femtosecond pump-supercontinuum probe setup described previously [13]. Briefly, a femtosecond colliding-pulse-modelocked dye laser oscillator generated 616 nm pulses with ~70 fs fwhm and 1–2 nJ energy/pulse. The beam was passed through a two-stage pulsed dye amplifier to generate pulses with 300–400 μJ energy/pulse and a repetition rate of 25 Hz. These pulses were compressed through a prism pair to compensate for the group-velocity dispersion in the amplification process. Then the beam was split off in two parts. One of them was frequency-doubled through a 0.5 mm KDP nonlinear crystal to produce 308 nm pump pulses with ~10 μJ energy/pulse. The other part was focused into a quartz cell with H_2O to generate supercontinuum probe pulses. The magic angle (54.7°) was set between the polarization of the pump and probe beams. The sample was circulated through a 1 mm quartz cell. After the sample, the supercontinuum was dispersed by a polychromator and detected by a photodiode array. Transient spectra $\Delta D(t, \lambda)$, where ΔD is change in optical density, were recorded over the ranges 400–580 and 650–900 nm; the spectral resolution was about 5 nm. The measured spectra were corrected for group delay dispersion of the supercontinuum using the procedure described previously [13]. Concentrations of samples were $\sim 1 \times 10^{-4}$ M. With 616 nm excitation, the concentrations of $[\mathbf{S}\cdot\mathbf{V}]^{4+}$ and $[\mathbf{S}\cdot\mathbf{V}\cdot\mathbf{S}]^{4+}$ were 7.5 and 4.5 mM, respectively.

The corrected transient spectra were analyzed using the global fitting procedure based on matrix self-modelling. This procedure allows a set of time-dependent spectra to be reconstructed from a single- or multi-exponential model. For example, assume that transient spectra vary according to the bi-exponential law

$$\Delta D(t,\lambda) = A_0(\lambda) + A_1(\lambda) \times \exp(-t/\tau_1) + A_2(\lambda) \times \exp(-t/\tau_2).$$

In matrix notation, this equation is presented as $\mathbf{D} = \mathbf{AE}$, where $\mathbf{D}$ is an $n \times m$ matrix containing the transient spectra measured at n different wavelengths and at m different delay times, $\mathbf{A}$ is an $n \times 3$ matrix whose columns are vectors $A_0(\lambda)$, $A_1(\lambda)$ and $A_2(\lambda)$, and $\mathbf{E}$ is a $3 \times m$ matrix, the first row of which is vector of ones, and the second and third rows are vectors $\exp(-t/\tau_1)$ and $\exp(-t/\tau_2)$, respectively. The matrix $\mathbf{E}$ is calculated by postulating values of τ_1 and τ_2, and then is used in conjugation with the experimental matrix $\mathbf{D}$ to generate a theoretical matrix $\mathbf{A}$ by the formula $\mathbf{A}' = \mathbf{DE}^{\mathrm{T}}(\mathbf{EE}^{\mathrm{T}})^{-1}$, where $\mathbf{E}^{\mathrm{T}}$ is the transpose of $\mathbf{E}$. A theoretical spectral matrix $\mathbf{D}$ is calculated as $\mathbf{D}' = \mathbf{A}'\mathbf{E}$. Then, the mean square deviation between the experimental matrix $\mathbf{D}$ and the reconstructed matrix $\mathbf{D}'$ is minimized by varying values of τ_1 and τ_2. If the supposed model is valid, the minimization simultaneously provides the time constants τ_1 and τ_2, the preexponential vectors $A_1(\lambda)$ and $A_2(\lambda)$, and the residual spectrum $A_0(\lambda)$. Global fitting was performed using standard MATLAB functions.

Molecular mechanics simulations of the supramolecular CT complexes $[\mathbf{S}\cdot\mathbf{V}]^{4+}$ and $[\mathbf{S}\cdot\mathbf{V}\cdot\mathbf{S}]^{4+}$ were done using the MMX force field, as implemented in the PCMODEL program [14].

3. Results and discussion

3.1. Steady-state spectroscopy

Steady-state absorption and emission data for the viologens $\mathbf{EV}^{2+}$ and $\mathbf{V}^{4+}$, the biscrown stilbene $\mathbf{S}$, and the CT complexes $[\mathbf{S}\cdot\mathbf{EV}]^{2+}$, $[\mathbf{S}\cdot\mathbf{V}]^{4+}$ and $[\mathbf{S}\cdot\mathbf{V}\cdot\mathbf{S}]^{4+}$ are collected in Table 1. The ground-state absorption spectra of $\mathbf{V}^{4+}$, $\mathbf{S}$, $[\mathbf{S}\cdot\mathbf{EV}]^{2+}$, $[\mathbf{S}\cdot\mathbf{V}]^{4+}$ and $[\mathbf{S}\cdot\mathbf{V}\cdot\mathbf{S}]^{4+}$ are represented in Fig. 1. The absorption spectrum of $\mathbf{EV}^{2+}$ was very similar to that of $\mathbf{V}^{4+}$.

Upon steady-state irradiation, the uncomplexed compounds $\mathbf{S}$, $\mathbf{V}^{4+}$ and $\mathbf{EV}^{2+}$ readily undergo the geometric *trans* → *cis* photoisomerization with the quantum yields 0.24, 0.37 and 0.40, respectively. The high reaction efficiency in solutions containing atmospheric oxygen suggests that the *trans* → *cis* photoisomerization of $\mathbf{S}$, $\mathbf{V}^{4+}$ and $\mathbf{EV}^{2+}$ proceeds via a singlet mechanism [15]. Prolonged irradiation of the viologens $\mathbf{V}^{4+}$ and $\mathbf{EV}^{2+}$ led to their degradation presumably due to oxidative photocyclization of the generated *cis*-isomers [16].

The initial *trans*-isomers of $\mathbf{S}$, $\mathbf{V}^{4+}$ and $\mathbf{EV}^{2+}$ fluoresce with the quantum yields 0.30, 0.020 and 0.016, respectively. In each case, the steady-state emission spectrum was close to a mirror image of the absorption spectrum.

Comparison of the steady-state spectroscopy data for $\mathbf{EV}^{2+}$ and $\mathbf{V}^{4+}$ shows that the terminal ammonium groups in $\mathbf{V}^{4+}$ have a minor effect on the spectroscopic and photochemical behaviour of this viologen vinylog.

Complexes $[\mathbf{S}\cdot\mathbf{EV}]^{2+}$, $[\mathbf{S}\cdot\mathbf{V}]^{4+}$ and $[\mathbf{S}\cdot\mathbf{V}\cdot\mathbf{S}]^{4+}$ exhibit a broad CT absorption band with a maximum ranging from 502 nm for $[\mathbf{S}\cdot\mathbf{V}]^{4+}$ to 527 nm for $[\mathbf{S}\cdot\mathbf{EV}]^{2+}$. The observed hypsochromic shift of the CT band of $[\mathbf{S}\cdot\mathbf{V}]^{4+}$ relative to that of $[\mathbf{S}\cdot\mathbf{EV}]^{2+}$ is attributable to a reduced donor strength of $\mathbf{S}$ in $[\mathbf{S}\cdot\mathbf{V}]^{4+}$, resulting from the electron withdrawal effect of the ammonium groups of $\mathbf{V}^{4+}$ bound to the crown ether fragments of $\mathbf{S}$ via hydrogen bonds.

Table 1
Steady-state spectroscopy data for compounds **S**, $\mathbf{EV}^{2+}$ and $\mathbf{V}^{4+}$, and CT complexes $[\mathbf{S}\cdot\mathbf{EV}]^{2+}$, $[\mathbf{S}\cdot\mathbf{V}]^{4+}$ and $[\mathbf{S}\cdot\mathbf{V}\cdot\mathbf{S}]^{4+}$[a]

Compound	λ_{max}^{abs} (nm)	ε_{max} ($mol^{-1}\,dm^3\,cm^{-1}$)	λ_{max}^{em} (nm)	φ_f[b]	φ_{t-c}[b]
$\mathbf{EV}^{2+}$	319	45 000	367	0.016	0.40
$\mathbf{V}^{4+}$	321	44 000	369	0.020	0.37
S	336	37 500	386	0.30	0.24
$[\mathbf{S}\cdot\mathbf{EV}]^{2+}$	527[c]	570[c]	–	–	–
$[\mathbf{S}\cdot\mathbf{V}]^{4+}$	502	390	–	$<10^{-4}$	–
$[\mathbf{S}\cdot\mathbf{V}\cdot\mathbf{S}]^{4+}$	519	1020	–	$<10^{-4}$	–

[a] In acetonitrile at ambient temperature.
[b] The fluorescence quantum yields, φ_f, and the quantum yields of *trans* → *cis* photoisomerization, φ_{t-c}, are measured to within about ±20%.
[c] Ref. [12].

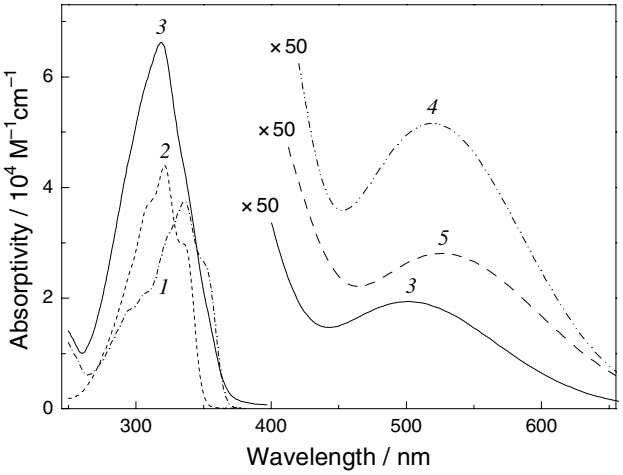

Fig. 1. Ground-state absorption spectra of **S** (1), $\mathbf{V}^{4+}$ (2), $[\mathbf{S}\cdot\mathbf{V}]^{4+}$ (3), $[\mathbf{S}\cdot\mathbf{V}\cdot\mathbf{S}]^{4+}$ (4), and $[\mathbf{S}\cdot\mathbf{EV}]^{2+}$ (5) in acetonitrile.

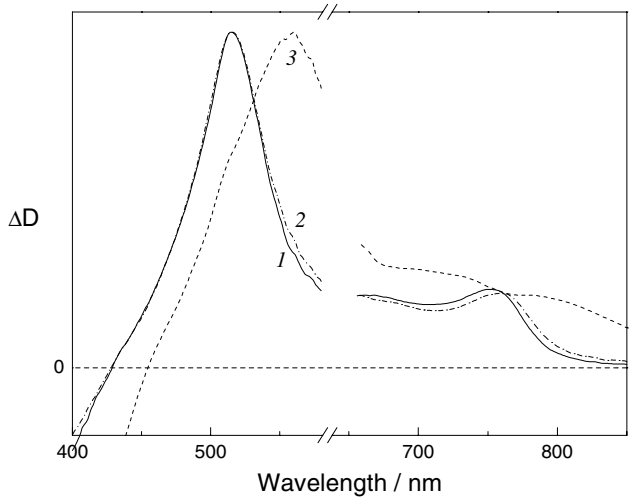

Fig. 2. Normalized transient absorption spectra of $\mathbf{V}^{4+}$ (1), $\mathbf{EV}^{2+}$ (2) and **S** (3) in acetonitrile. The spectra were measured 4 ps after excitation by a 308 nm, 70 fs laser pulse.

The CT complexes $[\mathbf{S}\cdot\mathbf{V}]^{4+}$ and $[\mathbf{S}\cdot\mathbf{V}\cdot\mathbf{S}]^{4+}$ unlike their components are nonfluorescent and do not undergo photoisomerization. This suggests that the CT excited states of $[\mathbf{S}\cdot\mathbf{V}]^{4+}$ and $[\mathbf{S}\cdot\mathbf{V}\cdot\mathbf{S}]^{4+}$ are rapidly deactivated via the back ET reaction.

3.2. Transient spectroscopy of $\boldsymbol{EV^{2+}}$, $\boldsymbol{V^{4+}}$ and **S**

Fig. 2 shows the normalized transient absorption spectra of $\mathbf{V}^{4+}$, $\mathbf{EV}^{2+}$ and **S** in acetonitrile. The spectra were measured 4 ps after excitation by a 308 nm, 70 fs laser pulse. In each case, the excitation wavelength falls into the region of the S_0–S_1 absorption band. Negative ΔD values at the short-wave edge of the transient spectra arise from stimulated emission. The transient absorption in the region 450–850 nm is due to electronic transitions from the fluorescent singlet state, S_1, to the higher-lying singlet states, S_N.

Viologens $\mathbf{EV}^{2+}$ and $\mathbf{V}^{4+}$ exhibit very similar $S_1 \rightarrow S_N$ absorption spectra. The maxima of the two clear-cut transient bands of $\mathbf{EV}^{2+}$ are around 515 and 759 nm. The low-energy transient band of $\mathbf{V}^{4+}$ is shifted hypsochromically by 6 nm relative to that of $\mathbf{EV}^{2+}$. The lowest singlet excited state of stilbene **S** shows a broad absorption band with the maximum at 560 nm and unstructured absorption between 650 and 850 nm.

Fig. 3 shows the transient absorption dynamics of $\mathbf{V}^{4+}$ on femto–picosecond timescale. The dynamics includes a significant rise between 120 and ~250 fs after the pump, blue shift and narrowing of the absorption bands in the interval from 120 fs to a few ps, and slow decay to a very weak residual signal.

Two sets of the transient absorption spectra of $\mathbf{V}^{4+}$ were simultaneously analysed using the global fitting procedure, as described in the Section 2. One of them included the transient spectra measured every 6.67 fs from 120 fs to 3.8 ps after the pump. Second set consisted of the transient spectra recorded every 0.667 ps from 0.667 to 190 ps after the pump. Both spectral sets were reconstructed rather well from a three-exponential kinetic model. Small deviations from this model were observed, however, on a 10 ps time scale. Best fit to transients was obtained using the four-exponential model

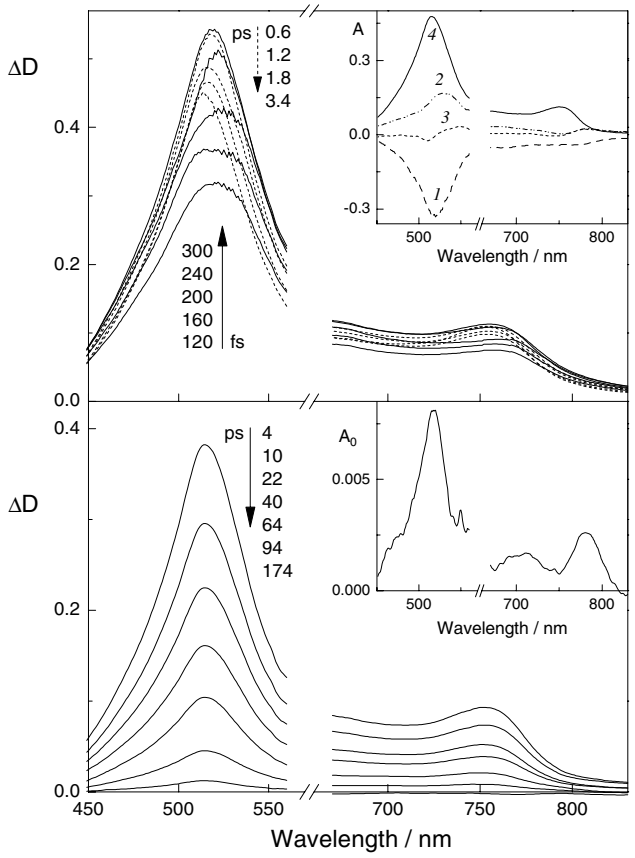

Fig. 3. Evolution of the transient absorption spectra of $\mathbf{V}^{4+}$ in acetonitrile after excitation by a 308 nm, 70 fs laser pulse. The upper inset shows the wavelength-dependent preexponential factors A_1–A_4 (curves 1–4, respectively) derived from the global fitting of the transient spectra to the four-exponential model $\Delta D(t,\lambda) = A_0(\lambda) + A_1(\lambda) \times \exp(-t/\tau_1) + A_2(\lambda) \times \exp(-t/\tau_2) + A_3(\lambda) \times \exp(-t/\tau_3) + A_4(\lambda) \times \exp(-t/\tau_4)$, with $\tau_1 = 89$ fs, $\tau_2 = 506$ fs, $\tau_3 = 10$ ps, and $\tau_4 = 43$ ps. The lower inset shows the residual spectrum A_0.

$$\Delta D(t,\lambda) = A_0(\lambda) + A_1(\lambda) \times \exp(-t/\tau_1) + A_2(\lambda) \times \exp(-t/\tau_2) + A_3(\lambda) \times \exp(-t/\tau_3) + A_4(\lambda) \times \exp(-t/\tau_4),$$

with $\tau_1 = 89$ fs, $\tau_2 = 506$ fs, $\tau_3 = 10$ ps, and $\tau_4 = 43$ ps. The preexponential vectors A_1–A_4 and the residual spectrum A_0 are represented in the insets in Fig. 3. The time plot of the transient absorption of $\mathbf{V}^{4+}$ at 515 nm on two different time scales is shown in Fig. 4.

The first three components of the transient dynamics of $\mathbf{V}^{4+}$ are attributable to relaxation processes in the S_1 excited state of $\mathbf{V}^{4+}$. The fitted τ_1–τ_3 values should be considered as crude estimates for the relaxation times because the first time constant is comparable with instrumental time resolution, and the spectral variations related to the third component are very small. The S_1 excited state lifetime for $\mathbf{V}^{4+}$ ($\tau_4 = 43$ ps) is measured to within about ±10%. The very weak residual spectrum A_0 resembles the ground-state absorption spectrum of 1,2-bis(*N*-benzyl-4-pyridiniumyl)ethylene radical cation

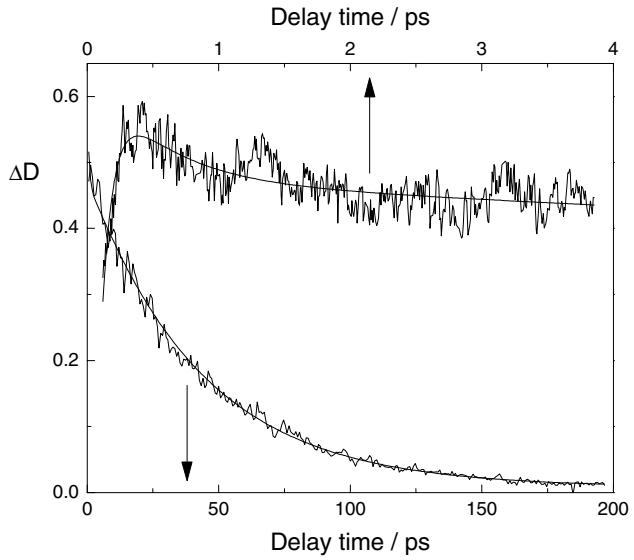

Fig. 4. Time plot of the transient absorption of $\mathbf{V}^{4+}$ at 515 nm in the intervals 0.12–3.8 and 0.67–190 ps; the smooth curves are from global fitting to the four-exponential model discussed in the text.

[17]. Therefore, this residual spectrum is tentatively assigned to the long-lived viologen radical cation resulting from two-photon reduction of $\mathbf{V}^{4+}$.

Recently, Zewail et al. [18] observed three-component relaxation in the lowest excited singlet state (Q(x) state) of free base tetraphenylporphyrin in benzene solution, which was assigned to intra- and intermolecular vibrational relaxation processes leading to thermal equilibrium in the Q(x) state. The time scales reported are as follows: 100–200 fs for intramolecular vibrational energy redistribution, 1.4 ps for vibrational redistribution caused by elastic collision with solvent molecules, and 10–20 ps for thermal equilibration by energy exchange with the solvent. We tentatively assume the same interpretation for the three-component relaxation in the S_1 excited state of $\mathbf{V}^{4+}$.

The transient absorption dynamics of the reference compound $\mathbf{EV}^{2+}$ was also described by a four-exponential kinetic model, but the spectral variations related to the second and third components of the relaxation in the S_1 excited state were even smaller than in the case of $\mathbf{V}^{4+}$. Therefore, we were unable to determine reliably the characteristic times for the relaxation processes in the S_1 excited state of $\mathbf{EV}^{2+}$. The deactivation of the S_1 excited state of $\mathbf{EV}^{2+}$ to the ground state was estimated to occur with a time constant of 31 ps.

The lowest singlet excited state of stilbene **S** showed a very long lifetime that is out of resolution of our experimental setup; the transient spectra of **S** measured between 200 and 600 ps were fit to a single-exponential decay model with a time constant of 1.1 ns.

Judging from the ground-state absorption spectra (Fig. 1 and Table 1), compounds **S**, $\mathbf{V}^{4+}$ and $\mathbf{EV}^{2+}$ should have comparable magnitudes of the oscillator

strength of the S_0–S_1 electronic transition and, hence, comparable rate constants of the radiative deactivation of the S_1 excited state. This assumption is in agreement with the fact that the order of increasing in the S_1 excited state lifetime, $\mathbf{EV}^{2+} < \mathbf{V}^{4+} \ll \mathbf{S}$, correlates with the order of increasing in the emission quantum yield (Table 1). The relatively short excited state lifetimes observed for $\mathbf{V}^{4+}$ and $\mathbf{EV}^{2+}$ are mainly due to very fast singlet *trans* → *cis* photoisomerization.

3.3. Excited state dynamics of CT complexes $[\mathbf{S}\cdot\mathbf{V}]^{4+}$ and $[\mathbf{S}\cdot\mathbf{V}\cdot\mathbf{S}]^{4+}$

Fig. 5 shows the evolution of the transient absorption spectra of the 1:1 complex $[\mathbf{S}\cdot\mathbf{V}]^{4+}$ between 120 fs and 3.5 ps after excitation in the CT absorption band by a 616 nm, 70 fs laser pulse. The transient absorption produced by the pump pulse decays to the base line in about 3 ps with discernible spectral reshaping between 120 and ~300 fs.

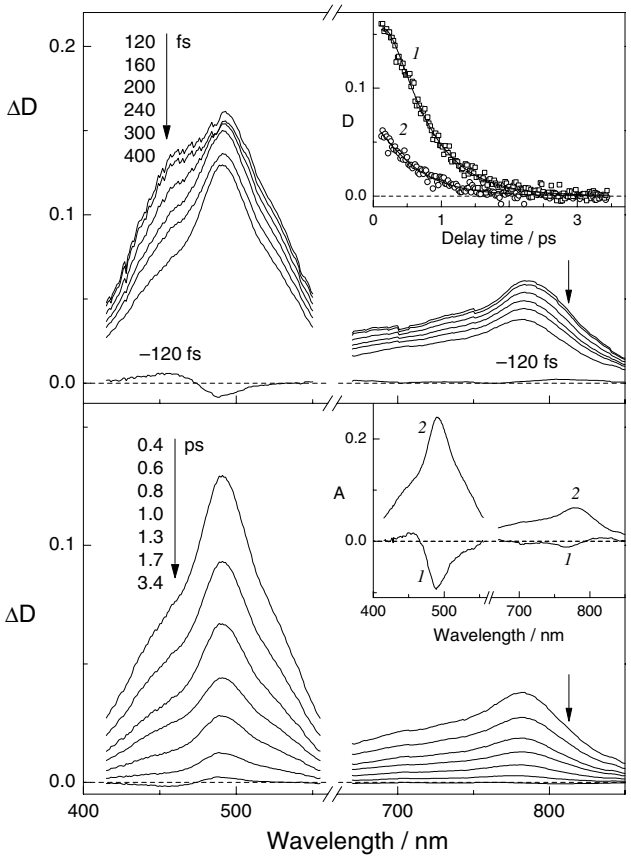

Fig. 5. Evolution of the transient absorption spectra of $[\mathbf{S}\cdot\mathbf{V}]^{4+}$ in acetonitrile after excitation by a 616 nm, 70 fs laser pulse. The upper inset shows the time plots of the transient signals at 491 (1) and 780 nm (2); the solid curves are from global fitting to equation $\Delta D(t,\lambda) = A_1(\lambda) \times \exp(-t/\tau_1) + A_2(\lambda) \times \exp(-t/\tau_2)$, with the time constants $\tau_1 = 170$ fs and $\tau_2 = 543$ fs. The lower inset shows the pre-exponential vectors A_1 (1) and A_2 (2).

The transient spectra of $[\mathbf{S}\cdot\mathbf{V}]^{4+}$ measured every 6.67 fs from 120 fs to 3.5 ps after the pump were analysed using the above-mentioned global fitting procedure. This analysis revealed that the spectra vary according to the bi-exponential law

$$\Delta D(t,\lambda) = A_1(\lambda) \times \exp(-t/\tau_1) + A_2(\lambda) \times \exp(-t/\tau_2),$$

with the time constants $\tau_1 = 170$ fs and $\tau_2 = 543$ fs. The wavelength-dependent preexponential factors A_1 and A_2 are represented in the lower inset in Fig. 5. The upper inset shows the time plots of the transient signals at 491 and 780 nm, i.e. at the absorption maxima in the spectrum A_2.

Excitation of $[\mathbf{S}\cdot\mathbf{V}]^{4+}$ in the CT absorption band leads directly to the lowest CT excited state, $[\mathbf{S}^+\cdot\mathbf{V}^-]^{4+}$, with nonequilibrium distribution of vibrational energy and nonequilibrium solvation. The ultrafast 170 fs transient observed with $[\mathbf{S}\cdot\mathbf{V}]^{4+}$ is attributable to relaxation processes in the lowest CT excited state. Because of instrumental errors, the measured τ_1 value should be considered as an estimate of the upper time limit for these processes. The 543 fs decay component is assigned to the deactivation of the relaxed CT excited state, $[\mathbf{S}^+\cdot\mathbf{V}^-]^{4+}|_{eq}$, to the ground state $[\mathbf{S}\cdot\mathbf{V}]^{4+}$ via the back ET reaction. The measurement accuracy for the ET time constant was estimated to be better than 10%.

In the supposed model of consecutive processes, $[\mathbf{S}^+\cdot\mathbf{V}^-]^{4+} \rightarrow [\mathbf{S}^+\cdot\mathbf{V}^-]^{4+}|_{eq} \rightarrow [\mathbf{S}\cdot\mathbf{V}]^{4+}$, the calculated spectra A_1 and A_2 have the following physical meaning. The first spectrum is a linear combination of the absorption spectra of $[\mathbf{S}^+\cdot\mathbf{V}^-]^{4+}$ and $[\mathbf{S}^+\cdot\mathbf{V}^-]^{4+}|_{eq}$, and the second one is the absorption spectrum of the relaxed CT excited state $[\mathbf{S}^+\cdot\mathbf{V}^-]^{4+}|_{eq}$.

Two-component transient dynamics has been observed previously with various organic D–A complexes [9,19–21]. The faster component is usually assigned to the relaxation of the excited complex from the Franck–Condon state to the equilibrated CT excited state. There are several pathways of the relaxation in the excited state, such as internal vibrational relaxation (IVR), solvent relaxation and vibrational cooling. The latter process is normally observed on a time scale from a few ps to a few tens ps. Therefore, it cannot account for the 170 fs transient observed with $[\mathbf{S}\cdot\mathbf{V}]^{4+}$. IVR process is less understood. It is generally assumed that IVR occurs much faster than vibrational cooling. The IVR in the excited state of hexamethylbenzene–tetracyanoethylene D–A complex was reported [22] to occur with a time constant of 115 fs. The time scale of 100–200 fs was recently measured for the IVR in the lowest excited singlet state of free base tetraphenylporphyrin in benzene [18]. One might expect that the IVR would reveal itself as a rise component in the transient absorption. As evident from the spectrum A_1, the relaxation from $[\mathbf{S}^+\cdot\mathbf{V}^-]^{4+}$ to $[\mathbf{S}^+\cdot\mathbf{V}^-]^{4+}|_{eq}$ leads not only to spectral reshaping but also to an increase in the integral ab-

sorption intensity, indicating the IVR effect. On the other hand, the time constant of the ultrafast relaxation corresponds with the longitudinal dielectric relaxation time of acetonitrile (170–180 fs [23]). Thus, both IVR and solvation dynamics can be responsible for the 170 fs transient. Unfortunately, insufficient instrumental time resolution did not allow us to assign this transient unambiguously.

From these observations, we can assume that the back ET reaction in the excited $[\mathbf{S}\cdot\mathbf{V}]^{4+}$ complex proceeds from fully equilibrated CT excited state. In that case, the semiclassical nonadiabatic ET theory may be applied to predict ET time. For organic D–A complexes, the single-mode quantum rate expression (Eq. (1), [24]) is commonly used.

$$\frac{1}{\tau_{ET}} = H_{RP}^2\sqrt{\frac{4\pi^3}{h^2\lambda_1 k_B T}}\sum_{n=0}^{\infty}\frac{S^n}{n!} \times \exp\left\{-S-\frac{(\Delta G_0+\lambda_1+nh\nu_a)^2}{4\lambda_1 k_B T}\right\}, \quad S=\frac{\lambda_2}{h\nu_a}, \tag{1}$$

where H_{RP} is the electronic coupling matrix element, ΔG_0 is the reaction Gibbs free energy, λ_1 is the reorganization energy associated with solvent and internal low-frequency modes, and λ_2 is the reorganization energy associated with a single averaged high-frequency internal mode of frequency ν_a.

The driving force ΔG_0 of the back ET in a D–A complex is commonly derived from electrochemical oxidation potential, E_{ox}, of the donor and reduction potential, E_{red}, of the acceptor using the relation

$$\Delta G_0 = E_{red}(A) - E_{ox}(D) + C, \tag{2}$$

where C is the Coulomb term. For bulky donor and acceptor molecules in highly polar solvent, the term C can be neglected [25]. Recently, it has been shown that strong host–guest interactions in the supramolecular CT complex $[\mathbf{S}\cdot\mathbf{V}]^{4+}$ affect significantly the redox properties of $\mathbf{S}$ and $\mathbf{V}^{4+}$ [26]. The oxidation potential of $\mathbf{S}$ and the reduction potential of $\mathbf{V}^{4+}$ are shifted upon complexation from 1.00 to 1.24 eV and from −0.50 to − 0.43 eV, respectively [26]. In this case, the electrochemical potentials of the complexed donor and the complexed acceptor are to be used in Eq. (2) to assess ΔG_0. Accordingly, the driving force for $[\mathbf{S}\cdot\mathbf{V}]^{4+}$ is estimated to be about −1.67 eV.

The matrix element H_{RP} can be estimated by the Hush formula [2,27]

$$H_{RP} = \frac{0.0206}{R}\sqrt{\nu_{max}\Delta\nu_{1/2}\varepsilon_{max}}, \tag{3}$$

where ν_{max}, $\Delta\nu_{1/2}$ and ε_{max} are the Gaussian parameters of the CT absorption band, and R is the ET distance. Deconvolution of the CT absorption band of $[\mathbf{S}\cdot\mathbf{V}]^{4+}$ gave $\nu_{max} = 19\,717$ cm^{-1} (2.44 eV), $\Delta\nu_{1/2} = 4878$ cm^{-1} (0.60 eV) and $\varepsilon_{max} = 375$ M^{-1} cm^{-1}. According to the MMX force field calculations of $[\mathbf{S}\cdot\mathbf{V}]^{4+}$, the stilbene fragment of $\mathbf{S}$ and the dipyridiniumyl ethylene fragment of $\mathbf{V}^{4+}$ have nearly planar geometry and lie in parallel planes at a distance of about 5 Å (Fig. 6). Assuming the ET distance in $[\mathbf{S}\cdot\mathbf{V}]^{4+}$ equal to the interplanar distance, we estimate the matrix element H_{RP} to be about 780 cm^{-1}.

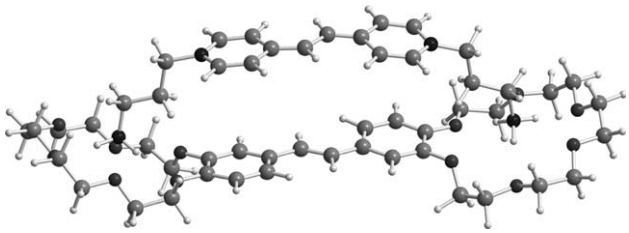

Fig. 6. Molecular mechanics model of the $[\mathbf{S}\cdot\mathbf{V}]^{4+}$ complex simulated using the MMX force field.

The total reorganization energy, $\lambda_0 = \lambda_1 + \lambda_2$, was predicted to be 0.77 eV using the relation $\lambda_0 = \Delta G_0 + \nu_{max}$. Following the common practice [28], the parameter ν_a was fixed at 1500 cm^{-1}. The reorganization energy λ_2 in Eq. (1) was varied to fit the calculated parameter τ_{ET} to the experimental ET time $\tau_2 = 543$ fs. The best fit was obtained when $\lambda_2 = 0.26$ eV. This value falls into the λ_2 interval of 0.2–0.4 eV assumed for organic D–A complexes [29], indicating the applicability of the nonadiabatic ET theory to this system.

It should be noted that the relaxed CT excited state $[\mathbf{S}^+\cdot\mathbf{V}^-]^{4+}|_{eq}$ has vibrational excess energy because the vibrational cooling, i.e. dissipation of the excess energy to the bath, occurs slower than the back ET reaction. In our calculations, we fixed T at 300 K, assuming that the internal temperature of the $[\mathbf{S}^+\cdot\mathbf{V}^-]^{4+}|_{eq}$ state is close to the bath temperature. This assumption is justified by the fact that the excitation at the red edge of the CT absorption band could not lead to a large vibrational excess energy. In addition, the vibrational excess energy of the $[\mathbf{S}^+\cdot\mathbf{V}^-]^{4+}|_{eq}$ state is distributed over a large number of internal modes.

In order to study the effect of vibrational excess energy on the back ET, the CT complex $[\mathbf{S}\cdot\mathbf{V}]^{4+}$ was excited at 308 nm. Fig. 7 shows the evolution of the transient spectra of $[\mathbf{S}\cdot\mathbf{V}]^{4+}$ in the interval from 120 fs to 3.5 ps after excitation by a 308 nm, 70 fs laser pulse. The pulse wavelength falls into the region of the most intense ground-state absorption of $[\mathbf{S}\cdot\mathbf{V}]^{4+}$ that is associated with the local electronic transitions of the complex components $\mathbf{S}$ and $\mathbf{V}^{4+}$. The excitation produces a transient absorption signal throughout the observed spectral range. The transient dynamics is more complicated in comparison with the previous case. It includes a significant rise between 120 and ~300 fs after the pump, noticeable spectral reshaping in the interval from 120 fs to ~0.5 ps, and a rapid decay between 0.5

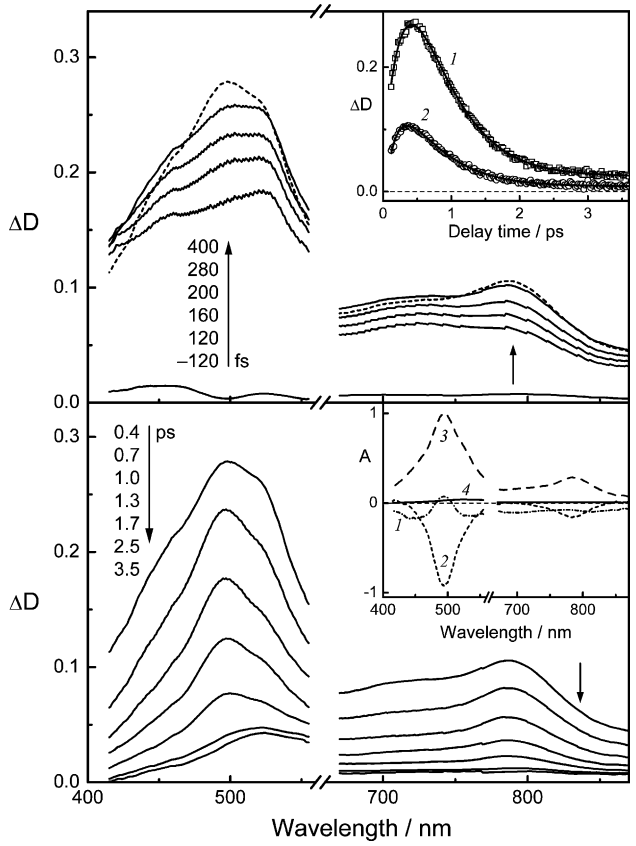

Fig. 7. Evolution of the transient absorption spectra of $[\mathbf{S}\cdot\mathbf{V}]^{4+}$ in acetonitrile after excitation by a 308 nm, 70 fs laser pulse. The upper inset shows the time plots of the transient signals at 495 (1) and 785 nm (2); the solid curves are from global fitting to equation $\Delta D(t,\lambda) = A_0(\lambda) + A_1(\lambda)\times\exp(-t/\tau_1) + A_2(\lambda)\times\exp(-t/\tau_2) + A_3(\lambda)\times\exp(-t/\tau_3)$, with the time constants $\tau_1 = 150$ fs, $\tau_2 = 295$ fs, and $\tau_3 = 536$ fs. The lower inset shows the preexponential vectors A_1–A_3 (curves 1–3, respectively) and the residual spectrum A_0 (4).

and 3.5 ps to a wavelength-dependent residual signal. The residual spectrum kept approximately its shape and intensity during at least a few tens ps.

The transient spectra measured every 6.67 fs from 120 fs to 3.5 ps after the pump were reconstructed well from the three-exponential model

$$\Delta D(t,\lambda) = A_0(\lambda) + A_1(\lambda)\times\exp(-t/\tau_1) + A_2(\lambda) \times\exp(-t/\tau_2) + A_3(\lambda)\times\exp(-t/\tau_3),$$

with the time constants $\tau_1 = 150$ fs, $\tau_2 = 295$ fs and $\tau_3 = 536$ fs. The lower inset in Fig. 7 shows the preexponential vectors A_1–A_3 and the residual spectrum A_0. The upper inset shows the time plots of the transient signals at 495 and 785 nm, i.e. at the absorption peaks in the spectrum A_3.

In the regions of the most significant spectral variations, the amplitudes of the dynamics components A_1–A_3 are much higher than the intensity of the residual signal A_0. This allows us to conclude that the appearance of this residual signal has insignificant effect on the time constant measurements.

The fastest 150 fs transient makes a relatively small contribution to the observed spectral dynamics. Presumably, it arises from relaxation processes in the high-lying excited states of the complex, mainly, in the locally excited states of the complex components. The 295 fs rise component is assigned to the internal conversion from the high-lying excited states to the lowest CT excited state. This assignment is consistent with the reported time constants of the S_N–S_1 internal conversion, 200–300 fs [30,31].

With 308 nm excitation, the IVR process in the lowest CT excited state $[\mathbf{S}^+\cdot\mathbf{V}^-]^{4+}$ is unobservable because it follows the slower process of the internal conversion. The 536 fs decay component is attributed to the deactivation of the relaxed CT excited state $[\mathbf{S}^+\cdot\mathbf{V}^-]^{4+}|_{eq}$ to the ground state $[\mathbf{S}\cdot\mathbf{V}]^{4+}$ via the back ET reaction. The absorption peaks of the $[\mathbf{S}^+\cdot\mathbf{V}^-]^{4+}|_{eq}$ state (spectrum A_3 in Fig. 7) are red-shifted by 4–5 nm relative to the corresponding peaks measured when the complex was excited at 616 nm (spectrum A_2 in Fig. 5). This shift is probably due to a large difference in the vibrational excess energy of the $[\mathbf{S}^+\cdot\mathbf{V}^-]^{4+}|_{eq}$ state. With neglect of the vibrational cooling process, this difference is determined to be 2.0 eV. Using the approximate approach reported in [30], we estimate the difference in the internal temperature of the $[\mathbf{S}^+\cdot\mathbf{V}^-]^{4+}|_{eq}$ state to be >120 K. With increasing T from 300 to 420 K, the ET time calculated by Eq. (1) decreases by ~23%, i.e. the nonadiabatic ET theory predicts a significant acceleration of the back ET for $[\mathbf{S}\cdot\mathbf{V}]^{4+}$ on changing the excitation wavelength from 616 to 308 nm. This prediction is at variance with our observation that the back ET time for $[\mathbf{S}\cdot\mathbf{V}]^{4+}$ is almost independent of excitation wavelength. It is unlikely that this discrepancy arises from experimental errors, as the measured ET time constants were well reproducible. Taking into account that the nonadiabatic ET model (Eq. (1)) neglects nonequilibrium reaction pathways, one may assume that this discrepancy is caused by nonequilibrium effects involving solvation or IVR. Such effects can play a significant role in ultrafast ET reactions [2].

The effect of solvent coordinate on the temperature dependence of the ET rate for $[\mathbf{S}\cdot\mathbf{V}]^{4+}$ can be estimated using the ET model introduced by Barbara and coworkers [7]. The time-dependent ET rate constant in this model is expressed as

$$k_{ET}(t) = H_{RP}^2\sqrt{\frac{4\pi^3}{h^2\lambda_{1v}k_BT}}\sum_{n=0}^{\infty}\frac{S^n}{n!} \times\exp\left\{-S-\frac{(\Delta G_0+\lambda_{1v}+[1-2X(t)]\lambda_s+nh\nu_a)^2}{4\lambda_{1v}k_BT}\right\},$$

$$S = \frac{\lambda_2}{h\nu_a}, \qquad (4)$$

where $X(t)$ is the solvent coordinate, λ_s is the solvent reorganization energy, and λ_{1v} is the reorganization energy associated with internal low-frequency modes. Note that the classical reorganization energy λ_1 of Eq. (1) is partitioned here into the two parts λ_s and λ_{1v}.

The solvent coordinate was introduced as $X(t) = 0.5 \times \exp(-t/\tau_s)$, where τ_s is the solvent relaxation time. The longitudinal dielectric relaxation time of acetonitrile (180 fs) was used for τ_s. The λ_{1v} value was fixed at 0.15 eV [7], and the average ET time $\tilde{\tau}_{ET}$ was calculated as follows [32]

$$\tilde{\tau}_{ET} = \int_0^\infty tQ(t)dt \Big/ \int_0^\infty Q(t)dt,$$
$$Q(t) = \exp\left\{ - \int_0^t k_{ET}(t)dt \right\}. \quad (5)$$

The energy λ_2 in Eq. (4) was varied to fit $\tilde{\tau}_{ET}$ to the experimental time constant. At $T = 300$ K, the best fit was found when $\lambda_2 = 0.35$ eV. The calculated $\tilde{\tau}_{ET}$ value decreased only by 7% with increasing T up to 420 K; i.e. the nonequilibrium ET model predicts smaller temperature dependence for the ET time. In this regard, it better describes the experimental data obtained for $[\mathbf{S}\cdot\mathbf{V}]^{4+}$. On the other hand, this model predicts strongly nonexponential ET kinetics, which is in conflict with the results of the global analysis of the transient absorption dynamics of $[\mathbf{S}\cdot\mathbf{V}]^{4+}$. The applicability of the nonadiabatic ET models (Eqs. (1) and (4)) to the $[\mathbf{S}\cdot\mathbf{V}]^{4+}$-type CT complexes should be tested in more detail. In particular, global analysis of spectral dynamics in terms of nonexponential kinetic models as well as measurements of the ET time as a function of the driving force would be useful.

Fig. 8 shows the evolution of the transient absorption spectra of the termolecular complex $[\mathbf{S}\cdot\mathbf{V}\cdot\mathbf{S}]^{4+}$ after excitation in the CT absorption band by a 616 nm, 70 fs laser pulse. The dynamics is qualitatively similar to that observed with the 1:1 complex $[\mathbf{S}\cdot\mathbf{V}]^{4+}$ (Fig. 5). Quantitative data on the dynamics were derived from the global analysis of two spectral sets. One of them included the transient spectra measured every 6.67 fs from 120 fs to 3.5 ps after the pump. Second set consisted of the transient spectra recorded every 20 fs in the interval from 120 fs to 8 ps. Both spectral sets were reconstructed well from the bi-exponential model

$$\Delta D(t,\lambda) = A_0(\lambda) + A_1(\lambda) \times \exp(-t/\tau_1) + A_2(\lambda) \times \exp(-t/\tau_2),$$

with the time constants $\tau_1 = 195$ fs and $\tau_2 = 1.08$ ps. The lower inset in Fig. 8 shows the calculated preexponential vectors A_1 and A_2. The upper inset shows the time curves of the transient signals at 494 and 795 nm, i.e. at the absorption peaks in the spectrum A_2.

The observed residual signal $A_0(\lambda)$ was very weak. It showed strong similarities to the long-lived transient

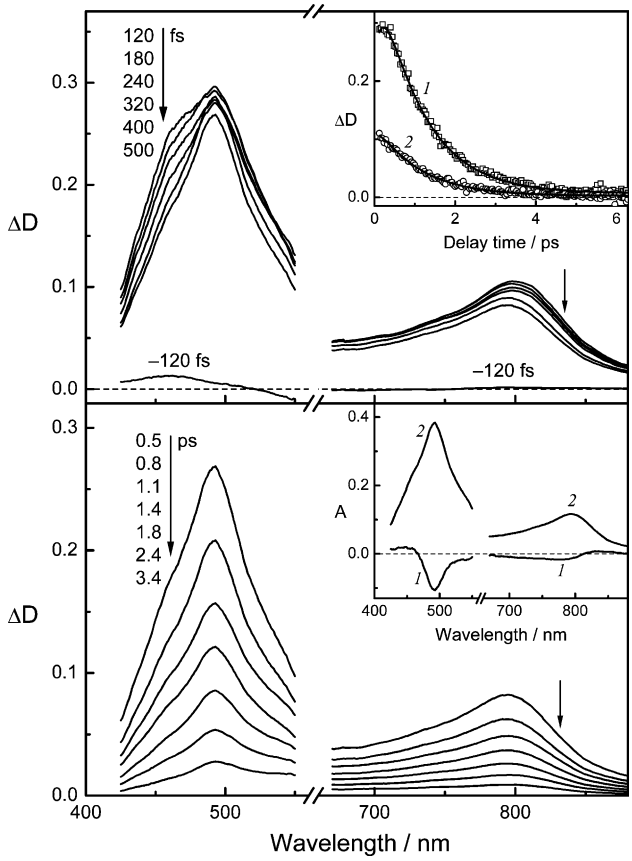

Fig. 8. Evolution of the transient absorption spectra of $[\mathbf{S}\cdot\mathbf{V}\cdot\mathbf{S}]^{4+}$ in acetonitrile after excitation by a 616 nm, 70 fs laser pulse. The upper inset shows the time plots of the transient signals at 494 (1) and 795 nm (2); the solid curves are from global fitting to equation $\Delta D(t,\lambda) = A_0(\lambda) + A_1(\lambda) \times \exp(-t/\tau_1) + A_2(\lambda) \times \exp(-t/\tau_2)$, with the time constants $\tau_1 = 195$ fs and $\tau_2 = 1.08$ ps. The lower inset shows the preexponential vectors A_1 (1) and A_2 (2).

spectrum of $\mathbf{S}$ (Fig. 2). The $[\mathbf{S}\cdot\mathbf{V}\cdot\mathbf{S}]^{4+}$ complex was excited in the presence of a large excess of $\mathbf{S}$ (0.05 M). Therefore, the residual signal is very likely to arise from two-photon excitation of the uncomplexed biscrown stilbene.

By analogy with the 1:1 complex, the faster component of the transient dynamics of $[\mathbf{S}\cdot\mathbf{V}\cdot\mathbf{S}]^{4+}$ is assigned to the relaxation processes in the lowest CT excited state $[\mathbf{S}^+\cdot\mathbf{V}^-\cdot\mathbf{S}]^{4+}$ leading to the relaxed CT excited state $[\mathbf{S}^+\cdot\mathbf{V}^-\cdot\mathbf{S}]^{4+}|_{eq}$. The latter is deactivated to the ground state via the back ET twice slower in comparison with the 1:1 complex. The absorption spectrum of the $[\mathbf{S}^+\cdot\mathbf{V}^-\cdot\mathbf{S}]^{4+}|_{eq}$ state (spectrum A_2 in Fig. 8) is similar in profile to that of $[\mathbf{S}^+\cdot\mathbf{V}^-]^{4+}|_{eq}$ (spectrum A_2 in Fig. 5). The most marked difference between these spectra lies in the 15 nm red shift of the long-wavelength band of $[\mathbf{S}^+\cdot\mathbf{V}^-\cdot\mathbf{S}]^{4+}|_{eq}$.

In the termolecular complex $[\mathbf{S}\cdot\mathbf{V}\cdot\mathbf{S}]^{4+}$, one of the crowns in each biscrown stilbene molecule is free of ammonium group. This fact suggests some decrease in

the oxidation potential of the complexed donor on going from $[S\cdot V]^{4+}$ to $[S\cdot V\cdot S]^{4+}$. Accordingly, one may assume some loss in the driving force of the ET reaction for $[S\cdot V\cdot S]^{4+}$. Using the Hush formula (Eq. (3)), the matrix element H_{RP} for $[S\cdot V\cdot S]^{4+}$ was estimated to be larger by a factor of 1.7 than that for $[S\cdot V]^{4+}$. To test the applicability of the nonadiabatic ET theory (Eq. (1)) to the termolecular CT complex $[S\cdot V\cdot S]^{4+}$, the parameter v_a was fixed at 1500 cm^{-1}, as with $[S\cdot V]^{4+}$, and the reorganization energy λ_2 was varied to fit the calculated ET time to the measured ET time constant 1.08 ps. Provided that $-\Delta G_0 < 1.67$ eV, the parameter λ_2 was estimated to be <0.15 eV; i.e. the semiclassical nonadiabatic ET theory predicts that the reorganization energy of high-frequency internal modes for $[S\cdot V\cdot S]^{4+}$ is considerably smaller than that for $[S\cdot V]^{4+}$.

Recently, Britt and McHale have studied Raman excitation profiles of a symmetrical D–A–D complex [33]. To rationalize some observations, they supposed that the CT excited state of this complex is delocalized due to adiabatic coupling of the two equivalent CT states D^+–A^-–D and D–A^-–D^+. In general, the electron delocalization in the CT excited state can affect both the external and the internal reorganization energies associated with the ET reaction. It may be suggested that the difference in the internal reorganization energy λ_2 between $[S\cdot V]^{4+}$ and $[S\cdot V\cdot S]^{4+}$ is related to the electron delocalization in the CT excited state of $[S\cdot V\cdot S]^{4+}$.

4. Summary

The supramolecular CT complexes $[S\cdot V]^{4+}$ and $[S\cdot V\cdot S]^{4+}$ show ultrafast two-component transient absorption dynamics in acetonitrile after excitation in the CT absorption band by a 616 nm, 70 fs laser pulse. The faster component ($\tau < 200$ fs) is tentatively attributed to vibrational relaxation processes in the lowest CT excited state. The second component is due to the back ET reaction leading to the ground state. For the $[S\cdot V]^{4+}$ complex, the measured ET time constant (about 540 fs) is in rather good agreement with the predictions of the semiclassical nonadiabatic ET theory (Eq. (1)). For the termolecular complex $[S\cdot V\cdot S]^{4+}$, the back ET reaction occurs twice slower, with a time constant of about 1.08 ps. The electronic coupling element H_{RP} for $[S\cdot V\cdot S]^{4+}$, as estimated by the Hush formula, is larger by a factor of 1.7 than that for $[S\cdot V]^{4+}$. Therefore it is rather difficult to justify the slower back ET rate for $[S\cdot V\cdot S]^{4+}$ on the basis of the nonadiabatic ET theory. Two quasi-degenerate CT excited states with electronic configurations close to $[S^+\cdot V^-\cdot S]^{4+}$ and $[S\cdot V^-\cdot S^+]^{4+}$ are expected for the termolecular CT complex. We tentatively suggest that the existence of these quasi-degenerate excited states is responsible for the relatively slow rate of the back ET reaction for the $[S\cdot V\cdot S]^{4+}$ complex. The experimental data available do not allow us to interpret this effect in more detail.

Excitation of the $[S\cdot V]^{4+}$ complex at the shorter wavelength 308 nm gives rise to three-component transient absorption dynamics. The fastest transient ($\tau \sim 150$ fs) is assigned to relaxation processes in the high-lying excited states of the complex. The high-amplitude rise component ($\tau \approx 300$ fs) is due to the internal conversion to the lowest CT excited state. The latter decays to the ground state via the back ET with a time constant very close to that measured when the complex was excited in the CT absorption band.

With 308 nm excitation, the back ET occurs from the relatively hot CT excited state, because the vibrational cooling process is much slower than this reaction. The internal temperature of this hot CT excited state was estimated to be more than 120 K higher than that expected with 616 nm excitation. Accordingly, the nonadiabatic ET theory predicts a significant acceleration of the back ET for $[S\cdot V]^{4+}$ on changing the excitation wavelength from 616 to 308 nm. This prediction is at variance with the observation. The nonequilibrium ET model of Barbara and co-workers (Eq. (4)) predicts smaller temperature dependence for the ET time. In this regard, it better describes the experimental data obtained for $[S\cdot V]^{4+}$. On the other hand, this model predicts nonexponential ET dynamics, which disagrees with the monoexponential ET kinetics derived from the global analysis of the transient absorption spectra of $[S\cdot V]^{4+}$.

In conclusion, the supramolecular CT complexes of the $[S\cdot V]^{4+}$ and $[S\cdot V\cdot S]^{4+}$ type can be utilized as convenient model systems for studies of ultrafast ET dynamics because of their high thermodynamic stability and rather well defined structure.

Acknowledgements

This work was supported by the RFBR (projects 02-03-32286 and 03-03-32178) and the INTAS (grant 2001-0267).

References

[1] R.A. Marcus, N. Sutin, Biochim. Phys. Acta 811 (1985) 265.
[2] P.F. Barbara, T.J. Meyer, M.A. Ratner, J. Phys. Chem. 100 (1996) 13148.
[3] R. Foster, Organic Charge-Transfer Complexes, Academic Press, New York, 1969.
[4] T. Asahi, N. Mataga, J. Phys. Chem. 93 (1989) 6575.
[5] T. Asahi, N. Mataga, Y. Takahashi, T. Miyashi, Chem. Phys. Lett. 171 (1990) 309.
[6] S.M. Hubig, T.M. Bockman, J.K. Kochi, J. Am. Chem. Soc. 118 (1996) 3842.

[7] G.C. Walker, E. Åkesson, A.E. Johnson, N.E. Levinger, P.F. Barbara, J. Phys. Chem. 96 (1992) 3728.
[8] P.F. Barbara, G.C. Walker, T.P. Smith, Science 256 (1992) 975.
[9] O. Nicolet, E. Vauthey, J. Phys. Chem. A 106 (2002) 5553.
[10] R.A. Denny, B. Bagchi, P.F. Barbara, J. Chem. Phys. 115 (2001) 6058.
[11] S.P. Gromov, E.N. Ushakov, A.I. Vedernikov, N.A. Lobova, M.V. Alfimov, Y.A. Strelenko, J.K. Whitesell, M.A. Fox, Org. Lett. 1 (1999) 1697.
[12] E.N. Ushakov, S.P. Gromov, A.I. Vedernikov, E.V. Malysheva, A.A. Botsmanova, M.V. Alfimov, B. Eliasson, U.G. Edlund, J.K. Whitesell, M.A. Fox, J. Phys. Chem. A 106 (2002) 2020.
[13] S.A. Antipin, A.N. Petrukhin, F.E. Gostev, V.S. Marevtsev, A.A. Titov, V.A. Barachevsky, Y.P. Strokach, O.M. Sarkisov, Chem. Phys. Lett. 331 (2000) 378.
[14] PCMODEL for Windows, Version 7.0, Serena Software.
[15] J. Saltiel, J. D'Agostino, E.D. Megarity, L. Metts, K.R. Neuberger, M. Wrighton, O.C. Zafiriou, in: O.L. Chapman (Ed.), Organic Photochemistry, Marcel Dekker, New York, 1973, p. V3.
[16] A.R. Gutierrez, D.G. Whitten, J. Am. Chem. Soc. 98 (1976) 6233.
[17] M. Nanasawa, M. Miwa, M. Hirai, T. Kuwabara, J. Org. Chem. 65 (2000) 593.
[18] J.S. Baskin, H.Z. Yu, A.H. Zewail, J. Phys. Chem. A 106 (2002) 9837.
[19] N. Mataga, in: J.R. Bolton, N. Mataga, G. McLendon (Eds.), Advances in Chemistry Series, ACS, 1991 (Chapter 6).
[20] I.R. Gould, D. Noukakis, L. Gomez-Jahn, R.H. Young, J.L. Goodman, S. Farid, Chem. Phys. 176 (1993) 439.
[21] W. Jarzeba, S. Murata, M. Tachiya, Chem. Phys. Lett. 301 (1999) 347.
[22] I.V. Rubtsov, K. Yoshihara, J. Phys. Chem. A 103 (1999) 10202.
[23] Y.Y. Akhadov, Dielectric parameters of pure liquids, MAI, Moscow, 1999 (in Russian).
[24] B.S. Brunschwig, N. Sutin, Comments Inorg. Chem. 6 (1987) 209.
[25] B.R. Arnold, S. Farid, J.L. Goodman, I.R. Gould, J. Am. Chem. Soc. 118 (1996) 5482.
[26] K.P. Butin, A.A. Moiseeva, S.P. Gromov, A.I. Vedernikov, A.A. Botsmanova, E.N. Ushakov, M.V. Alfimov, J. Electroanal. Chem. 547 (2003) 93.
[27] N.S. Hush, Prog. Inorg. Chem. 8 (1967) 391.
[28] M. Maiti, T. Misra, S. Sinha, S.K. Pal, D. Mukherjee, R.D. Saini, T. Ganguly, J. Lumin. 93 (2001) 261 (and references therein).
[29] C. Prayer, T.-H. Tran-Thi, S. Pommeret, P. d'Oliveira, P. Meynadier, Chem. Phys. Lett. 323 (2000) 467 (and references therein).
[30] K. Ohta, T.J. Kang, K. Tominaga, K. Yoshihara, Chem. Phys. 242 (1999) 103.
[31] H.H. Billsten, D. Zigmantas, V. Sundström, T. Polívka, Chem. Phys. Lett. 355 (2002) 465.
[32] H. Sumi, R.A. Marcus, J. Chem. Phys. 84 (1986) 4894.
[33] B.M. Britt, J.L. McHale, Chem. Phys. Lett. 270 (1997) 551.